R 753

Technical Report

POLYMER-IMPREGNATED CONCRETE SPHERICAL HULLS UNDER HYDROSTATIC LOADING

December 1971

Sponsored by

NAVAL FACILITIES ENGINEERING COMMAND

NAVAL CIVIL ENGINEERING LABORATORY

Port Hueneme, California 93043

Approved for public release; distribution unlimited

42

POLYMER-IMPREGNATED CONCRETE SPHERICAL HULLS UNDER HYDROSTATIC LOADING

Technical Report R-753

3.1610-1

by

H. H. Haynes and N. D. Albertsen

ABSTRACT

Eight spherical models with outside diameters of 16 inches and wall thicknesses of 1 or 2 inches were fabricated of polymer-impregnated concrete (PIC) having a uniaxial compressive strength of 21,000 psi. The spherical specimens were tested under hydrostatic loading conditions of short-term, long-term, and cyclic pressure. The test results show that the PIC spheres respond to hydrostatic loading with linearly elastic behavior and that the implosion pressures are greater by approximately 40% than those for similar regular-concrete spheres. Under short-term loading the specimens having a wall-thickness-to-outside-diameter ratio of 0.063 and 0.125 (1- or 2-inch walls to 16-inch OD) implode at average hydrostatic pressures of 4,810 and 8,475 psi, respectively. Classical elastic theory predicts the strain behavior and implosion pressures of the PIC sphere within engineering accuracy.

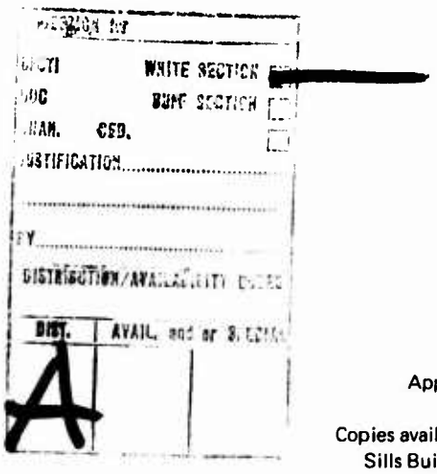

Unclassified
Security Classification

DOCUMENT CONTROL DATA - R & D

(Security classification of title, body of abstract and indexing annotation must be entered when the overall report is classified)

1. ORIGINATING ACTIVITY *(Corporate author)* Naval Civil Engineering Laboratory Port Hueneme, California 93043	2a. REPORT SECURITY CLASSIFICATION Unclassified 2b. GROUP

3. REPORT TITLE
POLYMER-IMPREGNATED CONCRETE SPHERICAL HULLS UNDER HYDROSTATIC LOADING

4. DESCRIPTIVE NOTES *(Type of report and inclusive dates)*
Final; June 1969 – February 1971

5. AUTHOR(S) *(First name, middle initial, last name)*
H. H. Haynes and N. D. Albertsen

6. REPORT DATE	7a. TOTAL NO. OF PAGES	7b. NO. OF REFS
December 1971	42	10

8a. CONTRACT OR GRANT NO.	9a. ORIGINATOR'S REPORT NUMBER(S)
b. PROJECT NO. 3.1610-1	TR-753
c.	9b. OTHER REPORT NO(S) *(Any other numbers that may be assigned this report)*
d.	

10. DISTRIBUTION STATEMENT
Approved for public release; distribution unlimited.

11. SUPPLEMENTARY NOTES	12. SPONSORING MILITARY ACTIVITY
	Naval Facilities Engineering Command Washington, D. C. 20390

13. ABSTRACT

Eight spherical models with outside diameters of 16 inches and wall thicknesses of 1 or 2 inches were fabricated of polymer-impregnated concrete (PIC) having a uniaxial compressive strength of 21,000 psi. The spherical specimens were tested under hydrostatic loading conditions of short-term, long-term, and cyclic pressure. The test results show that the PIC spheres respond to hydrostatic loading with linearly elastic behavior and that the implosion pressures are greater by approximately 40% than those for similar regular-concrete spheres. Under short-term loading the specimens having a wall-thickness-to-outside-diameter ratio of 0.063 and 0.125 (1- or 2-inch walls to 16-inch OD) implode at average hydrostatic pressures of 4,810 and 8,475 psi, respectively. Classical elastic theory predicts the strain behavior and implosion pressures of the PIC sphere within engineering accuracy.

DD FORM 1 NOV 68 1473 (PAGE 1)
S/N 0101-807-6801

Unclassified
Security Classification

Unclassified
Security Classification

14 KEY WORDS	LINK A		LINK B		LINK C	
	ROLE	WT	ROLE	WT	ROLE	WT
Polymer-impregnated concrete						
Monomers						
Regular concrete						
Concrete spheres						
Deep ocean structures						
Habitats						
Diallyl phthalate (DAP)						
Methyl-methacrylate (MMA)						
Polymerization						
Thermal-catalytic						
60 cobalt source						
Gamma radiation						
Hydrostatic pressure						
Short-term test						
Long-term test						
Cyclic test						
Aluminum joints						
Epoxy joints						
Strains						
Stresses						
Cost data						

CONTENTS

INTRODUCTION

The United States Navy and the United States Atomic Energy Commission (AEC) cosponsored this experimental program to investigate polymer-impregnated concrete (PIC) as a construction material for deep-ocean pressure-resistant structures. Polymer-impregnated concrete warranted investigation because its compressive strength, impermeability, and durability are greater than those of regular concrete. The Naval Civil Engineering Laboratory (NCEL) has been studying for the past 5 years the behavior of regular-concrete structures subjected to hydrostatic loading;[1-5] a natural extension to NCEL's research was to study PIC structures for underwater applications. The Division of Isotopes Development, AEC, has been promoting the development of PIC materials since the original concept was presented to them in 1965; their contribution to this research effort was to support the Brookhaven National Laboratory (BNL) in performing the impregnation and polymerization of the concrete test specimens.

The primary objective of the program was to experimentally investigate the structural behavior of PIC spheres subjected to various hydrostatic loadings and to determine tentatively the maximum operational depth for buoyant PIC spheres. A secondary objective was to compare PIC and regular-concrete materials when used in underwater structures.

Polymer-Impregnated Concrete (PIC)

Polymer-impregnated concrete (PIC) is precast portland cement concrete impregnated with a monomer system (plastic in a liquid or gaseous state) which is subsequently polymerized in situ. The resulting polymer system (plastic in a solid state) fills much of the voids in the concrete and, in so doing, acts both as a filler and a binder between cement paste and aggregate to improve the properties of the concrete. In general, the procedure employed to produce PIC materials is: precast, mature concrete is dried to constant weight; then the specimen is evacuated to remove air from the voids and soaked in a low viscosity liquid monomer until constant weight is attained. The specimen is wrapped in a vapor barrier to reduce evaporation

and finally placed in a chamber to polymerize the monomer. The two methods used most extensively to polymerize the monomer are gamma radiation from a cobalt 60 source and thermal catalytic processes.

Numerous monomer systems and their effect on the mechanical and physical properties of concrete have been investigated.[6-8] Compressive strengths greater than 20,000 psi and tensile strengths of 1,600 psi were obtained along with significant improvements in the durability properties; for example:

- Freeze–thaw durability increases of greater than 400%
- Chemical attack by sulfate brines reduced to negligible values
- Water permeability reduced to negligible values

Development work on PIC materials is in the early stages. Advances in PIC technology can be expected to improve further the properties of the material and to simplify the manufacturing techniques.

Pressure-Resistant Concrete Structures

Research at NCEL on the behavior of pressure-resistant concrete structures has been directed toward studying the response of the structure and the concrete material under hydrostatic pressure. The main objective of the research has been to develop the technology and design criteria necessary to accurately and safely utilize concrete as an underwater construction material for pressure-resistant structures.

Spherical and cylindrical model specimens have been tested; the major effort to date has been investigating spherical hulls having a 16-inch outside diameter and wall thicknesses of 1, 2, 3, or 4 inches. Test results have shown two stages of failure for the concrete spheres—development of cracks in the plane of the wall parallel to the major principal stresses, followed by implosion failure. Figure 1 compares graphically the pressures at in-plane cracking and implosion failure.[4]

TEST PROGRAM

Scope of Investigation

Eight 16-inch-OD spheres were tested under hydrostatic loading—six specimens had a 1-inch wall thickness and two specimens had a 2-inch wall thickness. Two types of monomers were used to make the polymer-impregnated

concrete: diallyl phthalate (DAP) which was polymerized by using a thermal catalytic process, and methyl-methacrylate (MMA) which was polymerized by using gamma radiation from a cobalt 60 source.

One of the 1-inch-thick specimens had an aluminum joint located at the equator which allowed the sphere to be separated into halves. The other specimens had a thin epoxy joint, approximately 1/32-inch thick, which bonded the two hemispheres together.

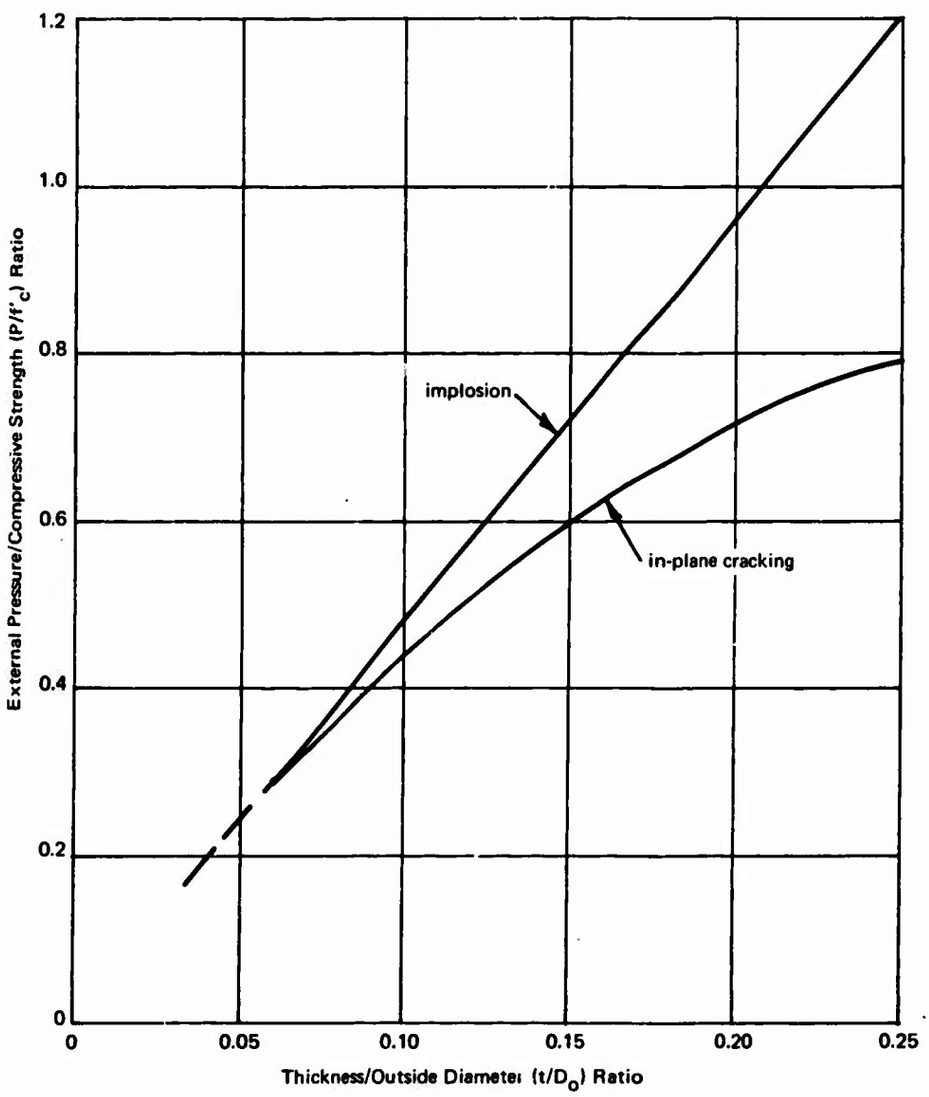

Figure 1. Comparison of failure modes for regular-concrete spheres subjected to hydrostatic loading.

Short-term, long-term, and cyclic hydrostatic loading conditions were imposed on different specimens in an effort to obtain data on the response of the PIC material to loading conditions which a real structure might undergo. Emphasis was placed on short-term tests so that comparisons in behavior could be made with existing data for regular-concrete spheres. The testing program is outlined in Table 1.

Table 1. Test Program

(Outside diameter of sphere was 16 inches.)

Sphere Description	Wall Thickness (in.)	Type of Monomer[a]	Monomer Load[b] (% by wt)	Type of Joint	Loading Condition
A	1	DAP	8.4	epoxy	short-term
B	1	DAP	7.9	epoxy	short-term
I	1	MMA	6.4	epoxy	short-term
C	2	DAP	9.0	epoxy	short-term
D	2	DAP	8.8	epoxy	short-term
F	1	DAP	8.0	aluminum	short-term
G	1	DAP	8.6	epoxy	long-term
H	1	DAP	8.0	epoxy	cyclic

[a] DAP = diallyl phthalate; 16.5-centipoise viscosity
MMA = methyl-methacrylate; 0.5-centipoise viscosity

[b] Average of two hemispheres.

Fabrication of Specimens

Fabrication of the specimens consisted of casting concrete hemispheres, curing the concrete, impregnating the concrete with a monomer to create polymer-impregnated concrete, and then joining together two hemispheres to form a sphere.

The concrete mix design given in Table 2 was the same as used in past studies on regular-concrete spheres. The concrete was moist-cured for the first 28 days and then stored at room conditions (for approximately 2 years) before it was impregnated with a monomer.

Six 3 x 6-inch control cylinders were cast with each hemisphere and cured under the same conditions as the hemisphere. Three control cylinders were used to obtain regular-concrete properties, and the other three cylinders were impregnated along with the hemisphere to obtain the PIC properties.

Even though the monomer impregnation and polymerization procedures (Table 3) were different for the DAP and MMA specimens, few problems were encountered in completely impregnating the concrete with either monomer. One problem encountered with the MMA impregnation procedure was that the monomer evaporated from the surface prior to polymerization. This resulted in a nonuniform monomer load in the wall of the hemispheres—the middle of the wall was completely impregnated, but the inner and outer wall surfaces had an 1/8-inch-thick layer that was lightly impregnated. Hemispheres 855B and 874B (sphere I) were re-impregnated in an attempt to raise the monomer load at the surfaces; the implosion results indicate the re-impregnation was successful. Subsequent to this experience, the monomer type was changed to DAP which is a less volatile monomer. Figure 2 shows a hemisphere section after impregnation with DAP.

Sphere F, which had a 1/4-inch-thick aluminum joint at the equator, is shown in Figure 3; Figure 4 is a cross-sectional view of the joint. The surface of the aluminum joint that mates with the concrete was beveled toward the center of the sphere at an included angle of $1^{o}50'$. The mating surfaces of the PIC hemispheres were machined to match the angle of the joint.

Each specimen, except for sphere I which had only two interior gages, was instrumented with at least 12 electrical resistance strain gages which were applied to the exterior and interior surfaces of one hemisphere. Figure 5 shows the typical gage layout.

Table 2. Concrete Mix Design

Water/cement ratio = 0.55 by weight

Aggregate/cement ratio = 3.30 by weight

San Gabriel River wash aggregate

Type III portland cement

Screen No.		Percent Retained
Passing	Retained	
4	8	29.6
8	16	20.8
16	30	14.7
30	50	10.3
50	100	7.3
100	pan	17.3

Table 3. Monomer Impregnation and Polymerization Procedure

Step in Process	Method Used for—	
	DAP Monomer	MMA Monomer
Drying of concrete	Oven dried to constant weight at 150°C	Oven dried to constant weight at 90°C
Evacuation of concrete	2 hr at a vacuum of 29 inches mercury	2 hr at a vacuum of 29 inches mercury
Monomer soak	16 hr at 20 psig	2 hr at 10 psig
Polymerization	Thermal-catalytic; 5% (by wt) of *t*-butyl perbenzoate catalyst; 110°C for 24 hr, plus 150°C for 150 hr	Gamma radiation from a 60 cobalt source; 250,000 rad/hr for 22 hr; total dose of 5.5×10^6 rad

Figure 2. Appearance of concrete hemisphere after impregnation with DAP monomer.

Figure 3. Assembly of sphere F with an aluminum joint.

Test Procedure

The specimens were tested under hydrostatic loading using freshwater as the pressure medium in NCEL's 18-inch-ID pressure vessel. Figure 6 shows a specimen attached to the pressure vessel head with a tubular steel penetrator vented outside the vessel. All the strain gage lead wires passed through this penetrator for hookup to data recording instruments.

Regardless of the type of test, pressure was applied to or removed from the specimen at a constant rate of 100 psi/min. Implosion of the specimen was easily noted by a sharp noise and instantaneous pressure drop.

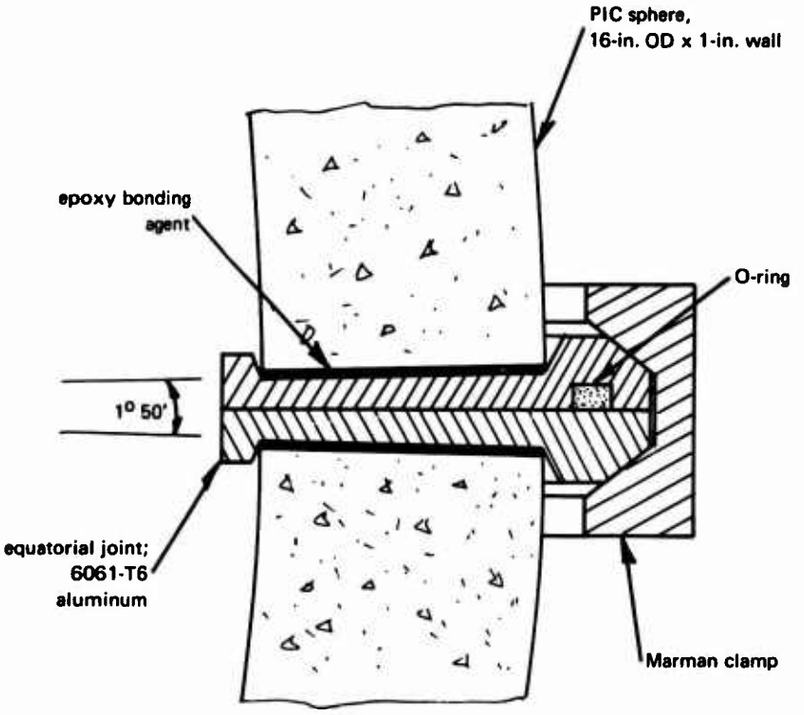

Figure 4. Cross-sectional view of aluminum joint.

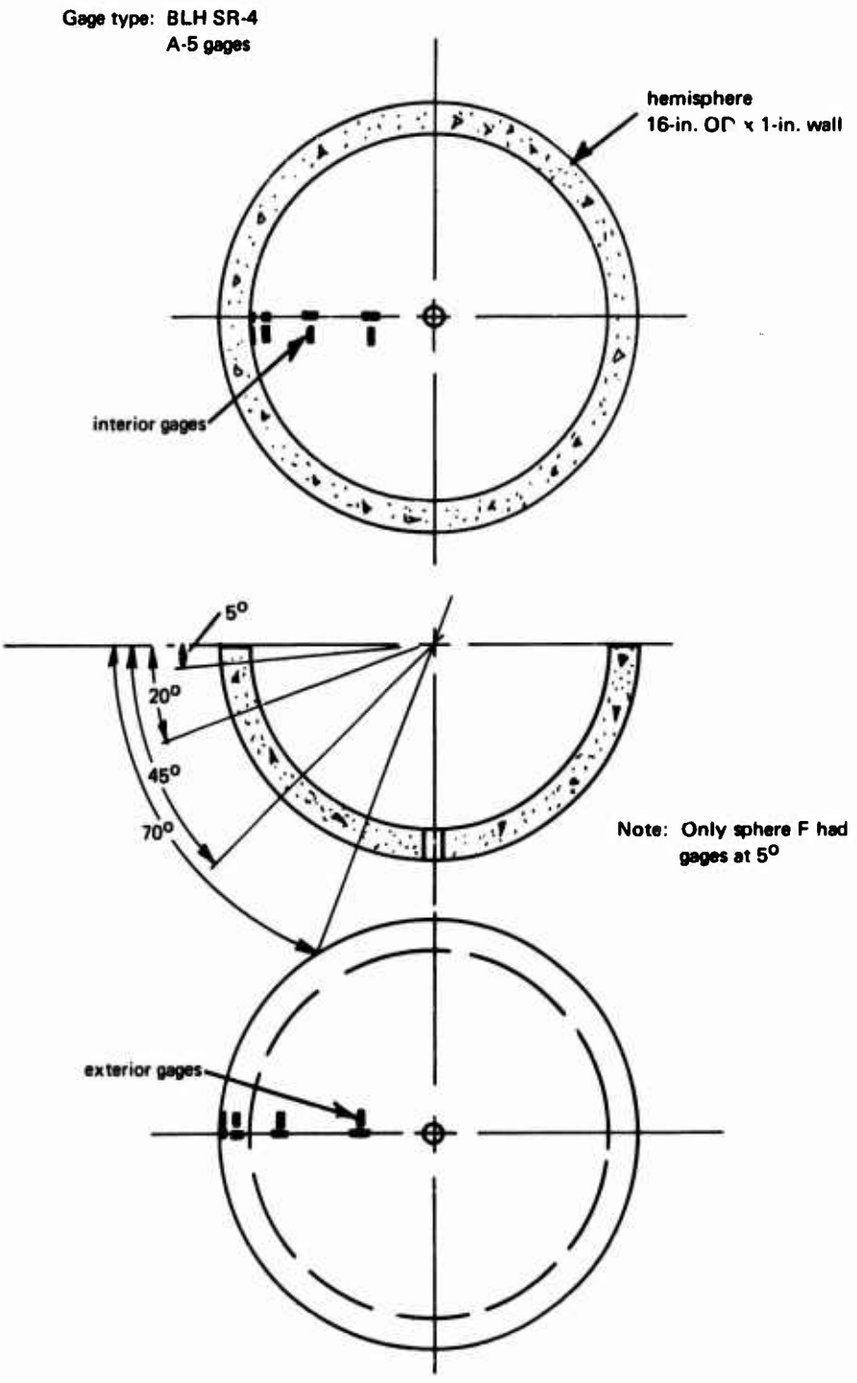

Figure 5. Typical strain gage layout for spheres.

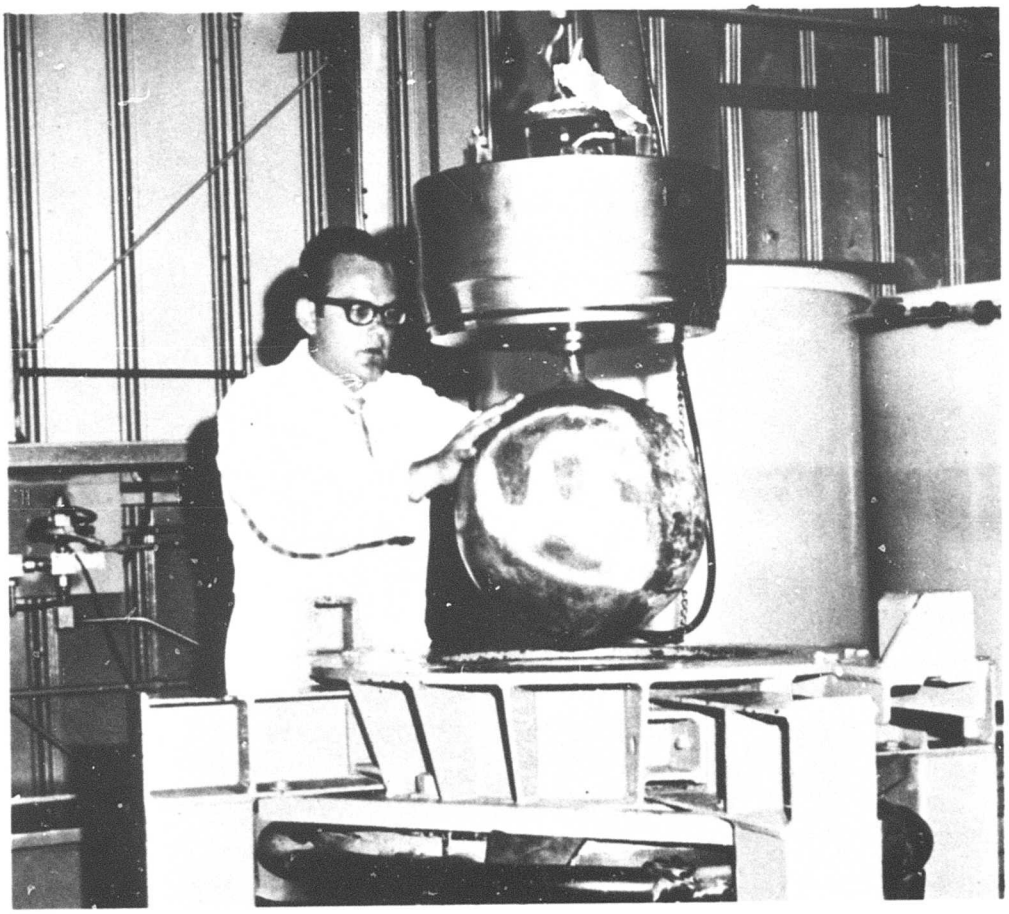

Figure 6. Specimen prepared for test in pressure vessel.

TEST RESULTS

Control Cylinder Tests

PIC and regular-concrete control cylinders were tested under uniaxial compression to determine compressive strength, modulus of elasticity and Poisson's ratio. Table 4 summarizes the results obtained from the 3 x 6-inch control cylinders. On the average, the PIC specimens contained 8.4% by weight DAP monomer, and exhibited an average compressive strength of 20,970 psi and a modulus of elasticity of 5.34×10^6 psi; these values were increases of 121 and 52%, respectively, over those of the regular-concrete control specimens. Poisson's ratio was found to be approximately the same, 0.17, for the PIC and regular-concrete specimens.

A typical stress–strain relationship for PIC and regular concrete is shown in Figure 7. These curves show the nearly linear behavior of PIC in comparison to the nonlinear behavior of regular concrete. The PIC material consistently showed elastic, brittle behavior under uniaxial compression.

Table 4. Test Data for 3 x 6-Inch Control Cylinder

Sphere Designation	Hemisphere No.	Type of Monomer	Monomer Load (% by wt)	Polymer-Impregnated Concrete			Regular Concrete			Increase in Compressive Strength (%)	Increase in Modulus of Elasticity (%)
				Compressive[a] Strength, f'_{PIC} (psi)	Modulus of[b] Elasticity, E (psi x 10^6)	Poisson's[b] Ratio, ν	Compressive[a] Strength, f'_c (psi)	Modulus of[b] Elasticity, E (psi x 10^6)	Poisson's[b] Ratio, ν		
A	724C 730C	DAP	8.2 8.7	21,550 20,960	5.16 4.76	0.16 0.23	9,750 9,940	– –	– –	121 111	– –
B	725C 731C	DAP	8.4 7.5	22,350 23,070	5.10 6.70	0.19 0.20	10,000 11,220	– –	– –	123 106	– –
I	855B 874B	MMA	6.7 6.1	20,060 21,300	7.50 7.10	0.27 0.23	8,740 8,740	3.80 3.80	0.17 0.17	130 144	97 87
C	963B 966B	DAP	9.0 9.1	21,200 21,000	4.82 5.19	0.13 0.21	8,110 8,720	3.00 3.35	0.17 0.24	161 141	61 55
D	435C 967B	DAP	9.0 8.7	19,950 20,000	5.00 4.53	0.16 0.14	9,200 8,070	3.62 2.79	0.14 0.12	117 148	38 62
F	721C 735C	DAP	7.8 8.2	20,800 20,500	5.36 5.72	0.14 0.19	10,050 10,050	– –	– –	107 104	– –
G	850B 890B	DAP	8.5 8.7	20,900 22,900	5.24 6.00	0.13 0.19	8,600 8,920	3.80 3.95	0.15 0.20	143 157	38 52
H	738C 751C	DAP	8.0 8.1	20,900 17,500	5.44 5.35	– 0.23	10,350 9,740	4.05 –	– –	102 80	34 –

[a] Average of three specimens.

[b] One specimen.

Short-Term Tests

Spheres A, B, I, C, and D were tested under short-term hydrostatic loading by applying pressure at a constant rate until implosion occurred; the implosion pressures for these spheres are given in Table 5.

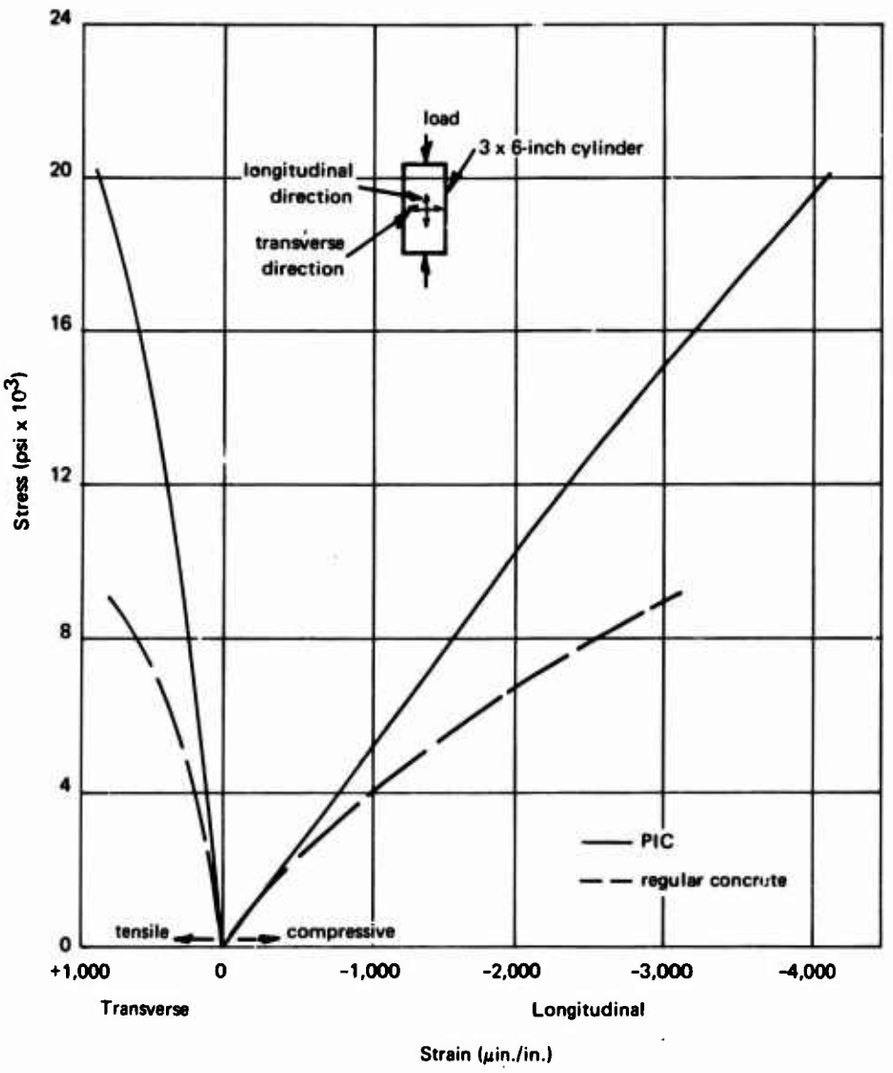

Figure 7. Typical stress—strain relationship for PIC and regular-concrete control cylinders under uniaxial compression.

Table 5. Implosion Results

Sphere Designation	Loading Condition	Wall Thickness (in.)	Uniaxial Compressive Strength, f'_{PIC} (psi)	Implosion Pressure, P_{im} (psi)	P_{im}/f'_{PIC}
A	short-term	1	20,960	4,670	0.222
B	short-term	1	22,350	5,065	0.226
I	short-term	1	20,060	4,700	0.234
C	short-term	2	21,000	8,750	0.417
D	short-term	2	19,950	8,200	0.411
F	short-term	1	20,500	4,130	0.202
G	long-term	1	20,900	4,000	0.191
H	cyclic	1	17,500	4,000	0.228

The average strain performance of the 1-inch-thick specimens, spheres A, B, and I, is shown in Figure 8 along with the performance of a previously tested regular-concrete sphere.[1] These curves show the striking differences in behavior between the PIC and regular-concrete spheres. One significant difference was the linear response of the PIC spheres to increasing hydrostatic pressure as opposed to the typical nonlinear behavior of regular concrete. Another difference was the pressure at which PIC spheres imploded—an average pressure of 4,810 psi. This was 43% higher than regular-concrete spheres, whose implosion pressure was predicted from an empirical equation developed in Reference 4.

The 2-inch-thick PIC specimens, spheres C and D, imploded at an average pressure of 8,475 psi, which was an increase of 36.5% over regular concrete. The strain performance of these spheres is shown in Figure 9; again the linear pressure–strain behavior was prevalent.

Sphere C unintentionally underwent two load cycles. The first cycle reached 84% of the actual implosion pressure before the pressure accidently decreased to zero at a rate of approximately 5,000 psi/min because of mechanical difficulties with the pressure vessel equipment. After a 10-minute delay, the second cycle was commenced and progressed to the implosion level. The slope of the pressure–strain curve for the second cycle increased approximately 7% over that of the first cycle. Also, during the second cycle the slope of the curve increased slightly with load up to implosion; in other words, the sphere became slightly stiffer with increased load.

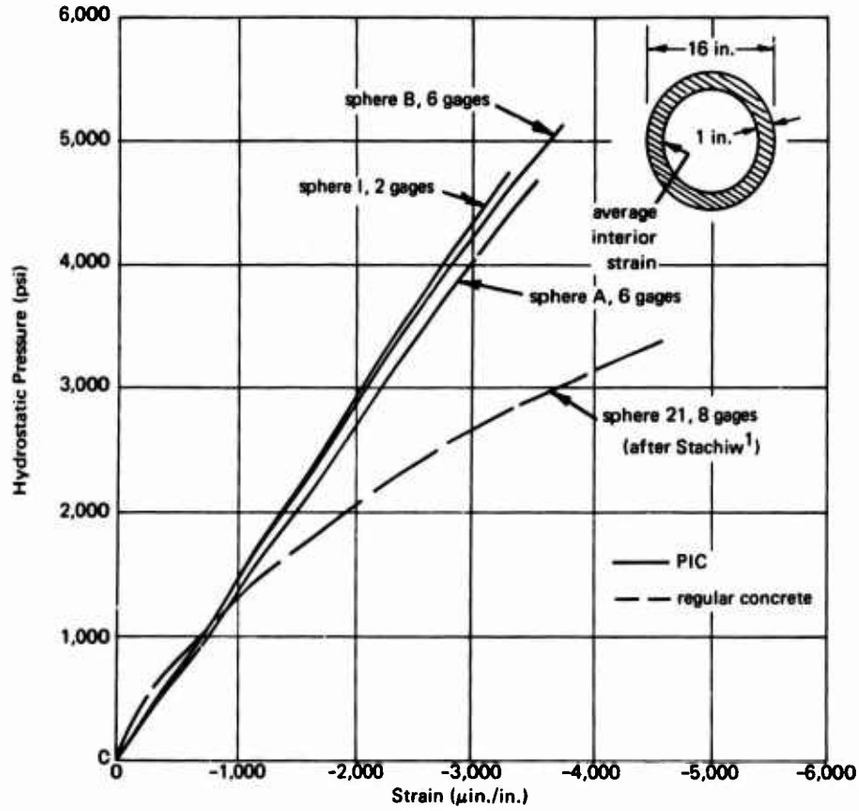

(a) Interior.

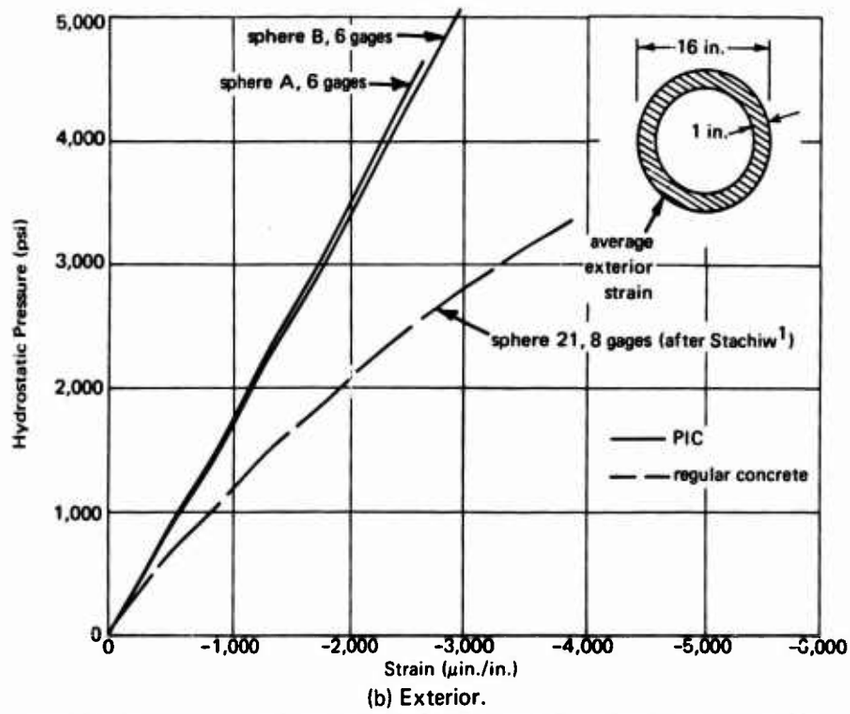

(b) Exterior.

Figure 8. Strain behavior of spheres subjected to short-term loading; $t/D_o = 0.063$.

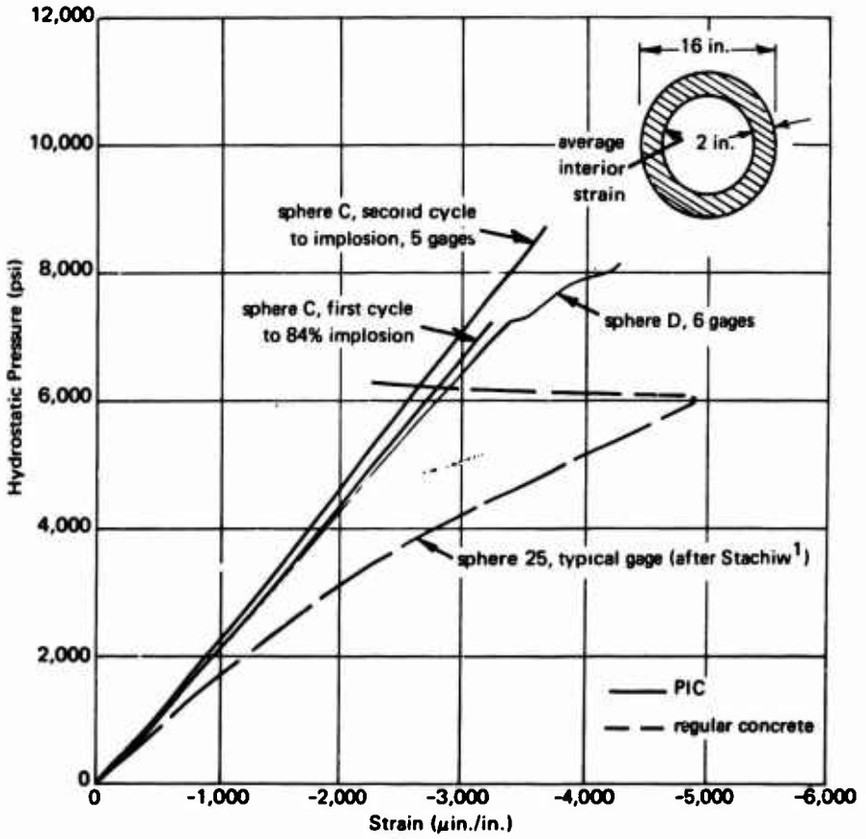

(a) Interior.

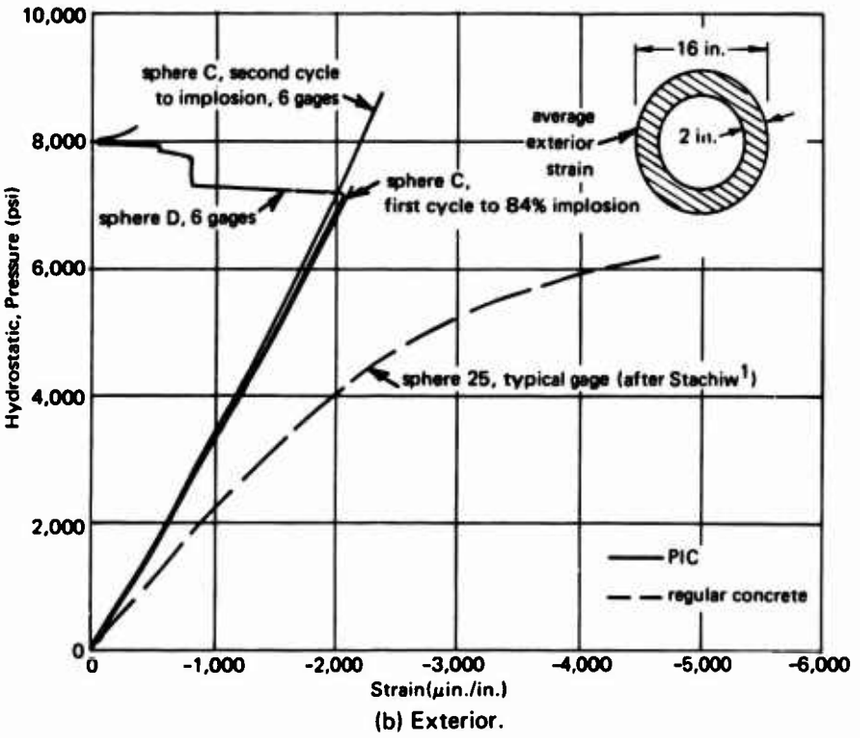

(b) Exterior.

Figure 9. Strain behavior of spheres subjected to short-term loading; $t/D_o = 0.125$.

Sphere D exhibited in-plane cracking* similar to regular-concrete spheres,[4] except cracking began at or near the exterior surface whereas the regular-concrete spheres cracked near the interior surface. The pressure at initiation of in-plane cracking, P_{pl}, was taken at the pressure where the strains (interior or exterior) were maximum before decreasing in value; for sphere D, P_{pl} was 7,200 psi. Figure 10 shows a fragment of sphere D after implosion which portrays these cracks. It was apparent from studying the individual gage data, Figure 11, that the in-plane cracks developed near the epoxy joint and propagated away from the joint. A plausible explanation for in-plane cracking is that the epoxy material at the joint is under a compressive stress of approximately 19,000 psi; at such high compressive stresses the tangent modulus of elasticity for epoxies is known to be quite low. The epoxy would

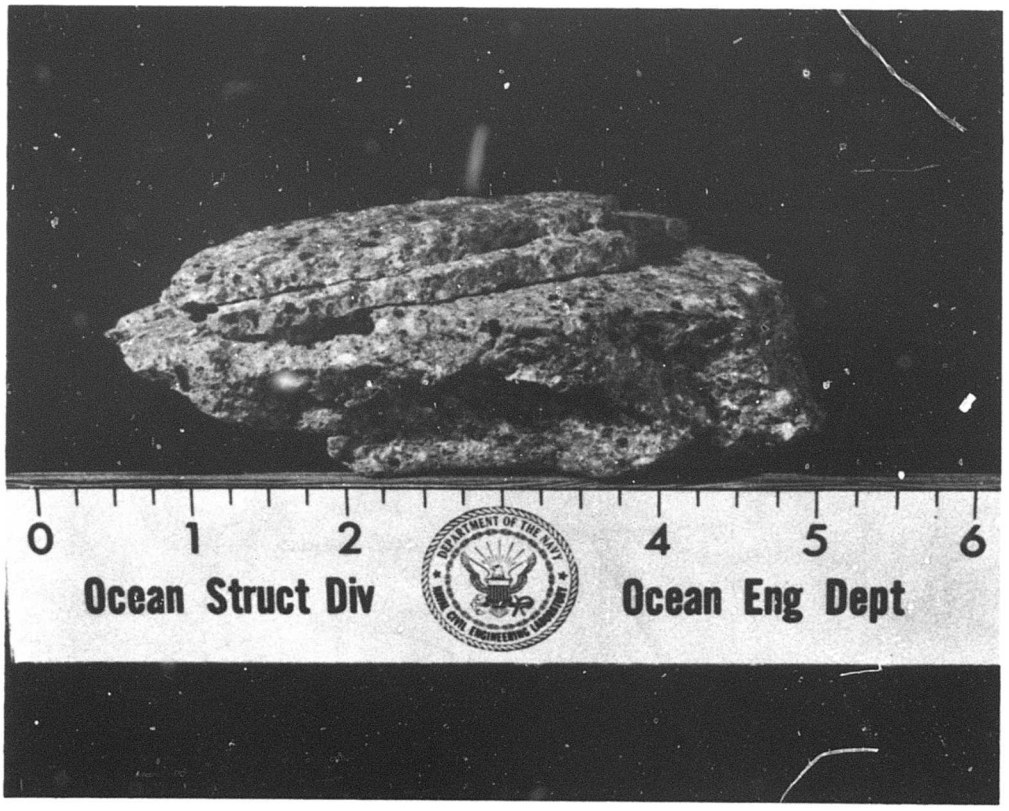

Figure 10. Fragment of sphere D showing in-plane cracks.

* In-plane cracking is the development of cracks in the concrete wall parallel to the major principal stresses, hence, cracking "in-the-plane" of the wall.

tend to extrude from the joint and, in so doing, would create tensile radial strains; these would add to the "normal" tensile strains already existing in the wall (300 μin./in. at 7,200 psi according to elastic theory). Thus, in-plane cracks could begin at the joint near the exterior wall as found in sphere D or near the interior wall as found in regular-concrete spheres.

Table 6 compares the uniaxial compressive strength, f'_{PIC}, of PIC control cylinders with the calculated interior wall stress at implosion, σ_{im}, for the PIC spheres. The interior surface of the spheres was under biaxial loading conditions where the tangential stresses were equal and the radial stress was zero. The tangential wall stress at implosion increased approximately 4% over the uniaxial compressive strength; this was a small increase compared to that of regular concrete which increased approximately 35%.[4] Hence, the PIC material did not show the improved strength under biaxial loading that was characteristic of regular concrete.

Table 6. Tangential Wall Stress at Implosion

Sphere Designation	Wall Thickness (in.)	Uniaxial[a] Compressive Strength, f'_{PIC} (psi)	Stress at Implosion, σ_{im} (psi)	σ_{im}/f'_{PIC}
A	1	20,960	21,250[b]	1.01
B	1	22,350	23,045[b]	1.03
I	1	20,060	21,385[b]	1.07
C	2	21,000	22,750[b]	1.08
D	2	19,950	18,720[c]	0.94

[a] For 3 x 6-inch control cylinders corresponding to the weaker hemisphere in the sphere.

[b] On interior wall of sphere; calculated using elastic theory, Equation 2.

[c] At in-plane cracking; calculated using Equation 2.

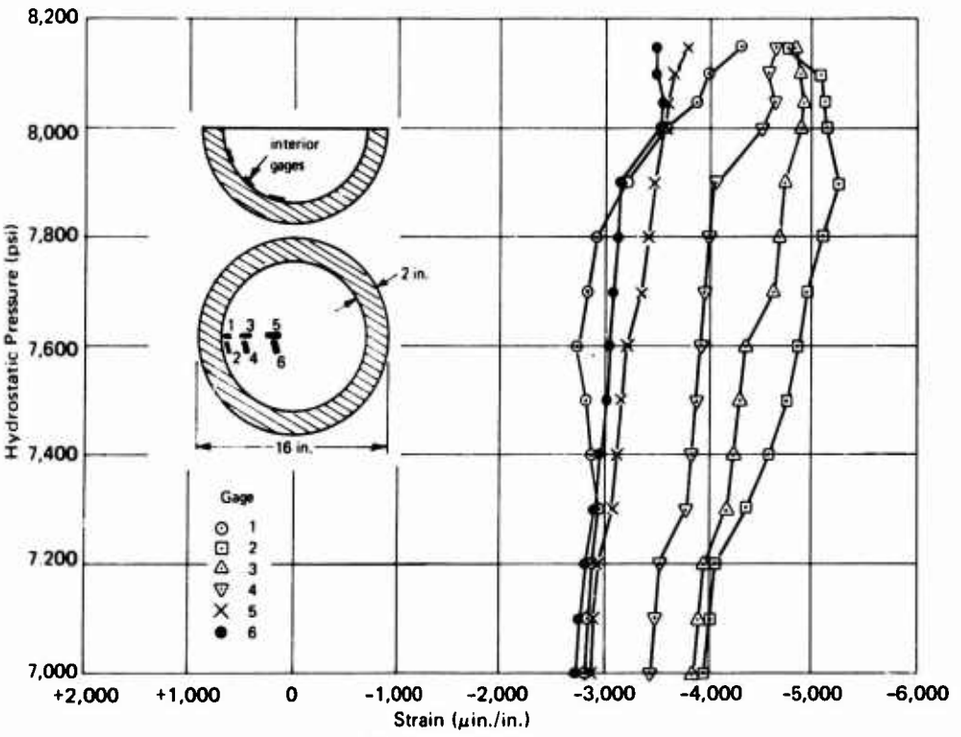

(a) Interior gages.

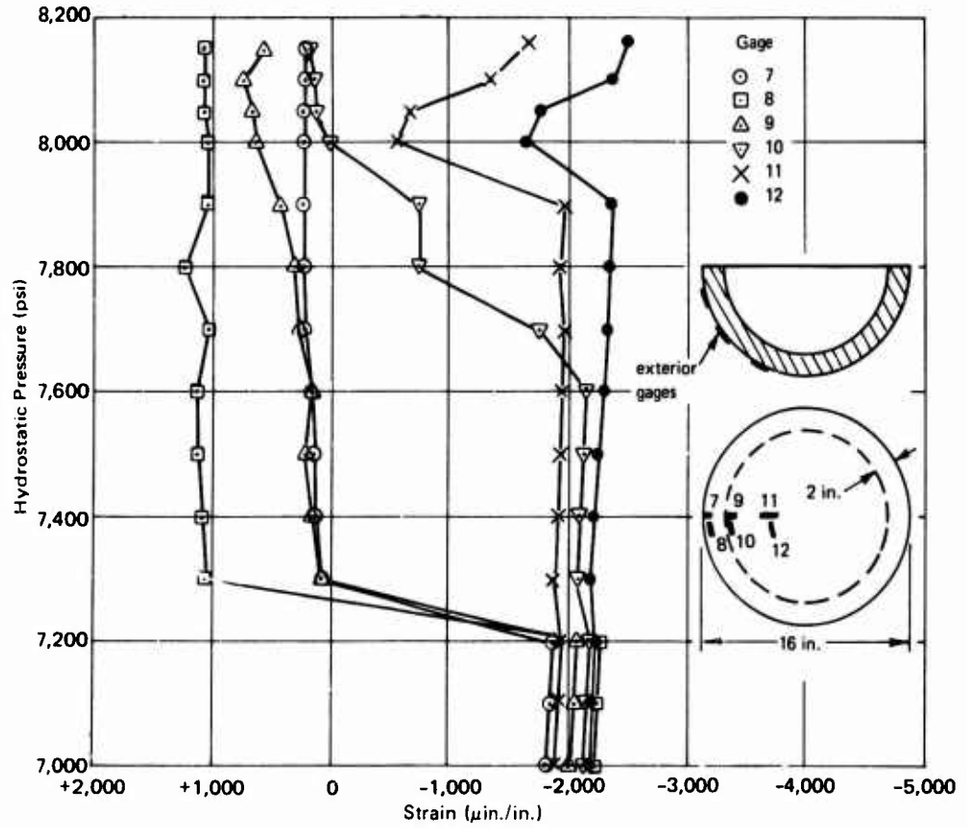

(b) Exterior gages.

Figure 11. Behavior of individual gages at in-plane cracking of sphere D.

Long-Term Test

Sphere G was tested under long-term loading where the pressure load was held constant for 100-hour periods at successively increasing 1,000-psi increments. Implosion occurred 3 minutes after reaching the 4,000-psi level; this pressure was 82% of the average implosion pressure for PIC spheres tested under short-term loading.

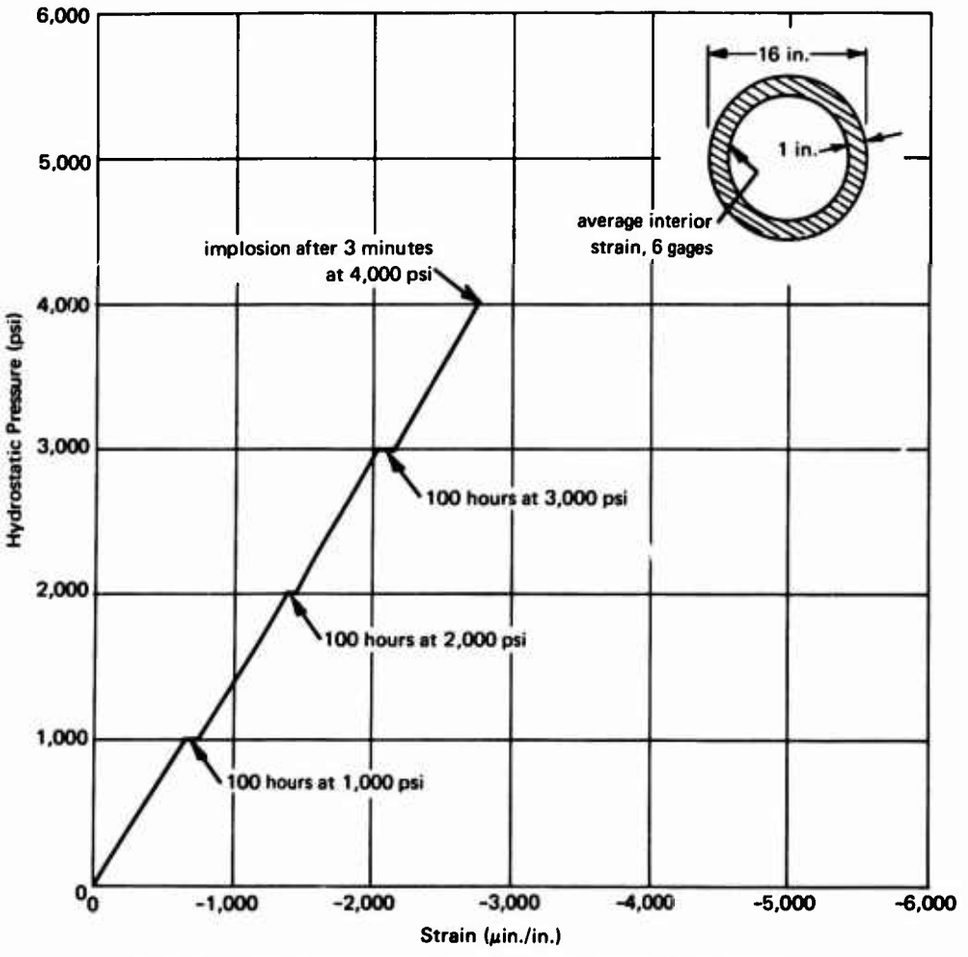

Figure 12. Interior strain versus hydrostatic pressure for sphere G under long-term loading; $t/D_o = 0.063$.

Figure 12 shows the strain performance of the specimen under the long-term loading sequence as a function of hydrostatic pressure. The specimen exhibited linear strain behavior between the constant pressure levels, and the secant slope to failure of the pressure–strain curve was almost identical to that exhibited by the PIC specimens under short-term loading. In addition,

the slope of the pressure–strain curve between sustained pressure levels became slightly steeper with higher pressure, indicating that the polymer-impregnated concrete became stiffer with time under load.

Figure 13 shows the strain performance of the specimen under long-term loading as a function of time. At 3,000 psi the specimen showed an increase in creep strain of approximately 100 μin./in. for the 100-hour duration of the load. Previous studies on similar regular-concrete spheres[1] indicated that sustained pressure loads of 1,500 psi produced several times this amount of creep strain for the same time interval.

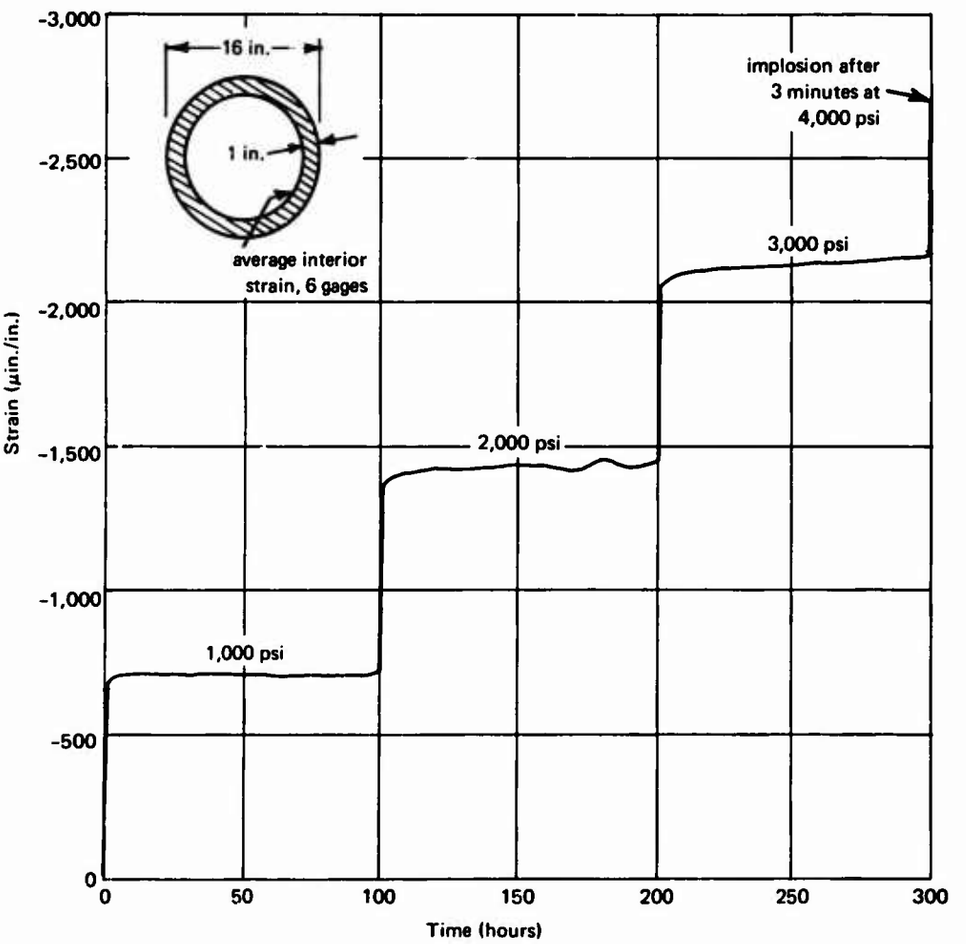

Figure 13. Interior strain versus time for sphere G under long-term loading; $t/D_o = 0.063$.

Cyclic Test

Sphere H was tested under cyclic loading where the pressure load was held constant for 50 hours followed by zero pressure for 50 hours at successively increasing 1,000-psi increments. The test simulated a set of placement–retrieval cycles that a structure might undergo during actual operating conditions.

Figure 14 shows the average interior and exterior strain performance of the specimen under cyclic loading as a function of hydrostatic pressure. These figures again illustrate the linear strain behavior of PIC spheres and the small amount of creep strain at each load level. Also, when the load was decreased at the rate of 100 psi/min, the sphere responded with linearly diminishing strain until, at zero load, the strain values were near zero. This behavior indicates that PIC is an elastic material which recovers from sustained loading with only small residual effects. In contrast, Figures 15 and 16 show that a regular-concrete sphere responded to one cycle of 67 hours at 3,000 psi with approximately 600 μin./in. of residual compressive strain.

Figure 17 illustrates the average interior and exterior strain performance of sphere H as a function of time. These figures show that during the no-load portion of each cycle the sphere displayed strain recovery into the positive strain range. This phenomenon, which has been observed by other investigators studying PIC materials, is not fully understood, but a proposed hypothesis is that an applied stress may induce a monomer phase change which results in an increased unit volume.[6]

Implosion of sphere H occurred after 15 minutes at 4,000 psi, which was the same implosion pressure and nearly the same time to implosion as that experienced in the long-term test, sphere G. This indicates that differences in extended loading conditions may have little effect on the implosion strength of the specimens—a quality which will be important to structures in actual use because of the implied predictability of the PIC material.

Although no direct measurements of the hull's watertightness were taken, a reliable indicator of watertightness is the degree to which the external pressure remains constant during a sustained load period. For both spheres G and H the indications were that the hulls were highly watertight.

Test of Sphere With Aluminum Joint

Sphere F with a mechanical aluminum joint located at the equator was tested under short-term loading to determine the effect of the joint on the behavior of the sphere.

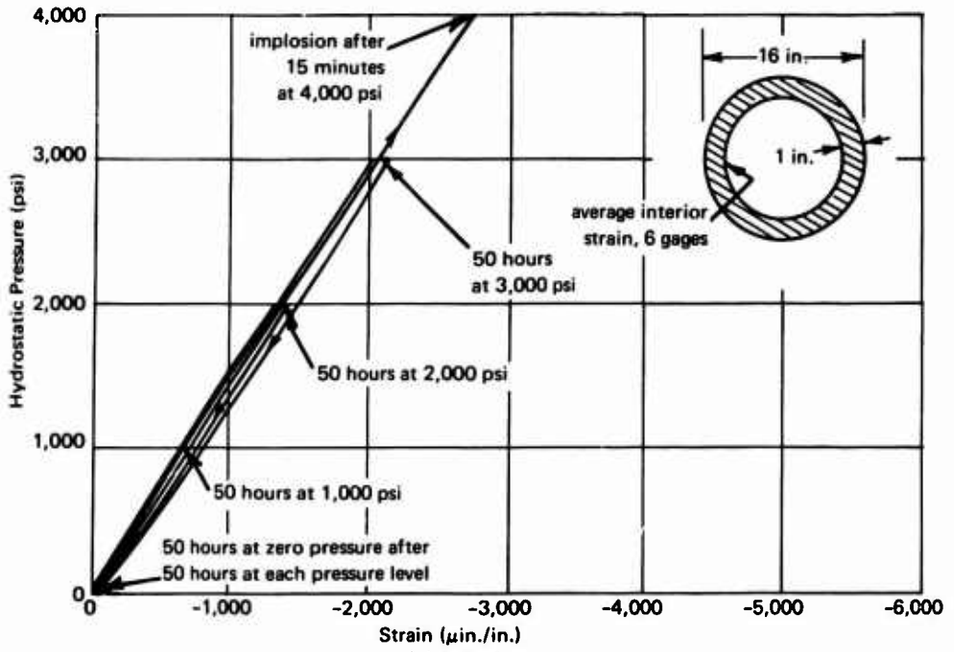

(a) Interior.

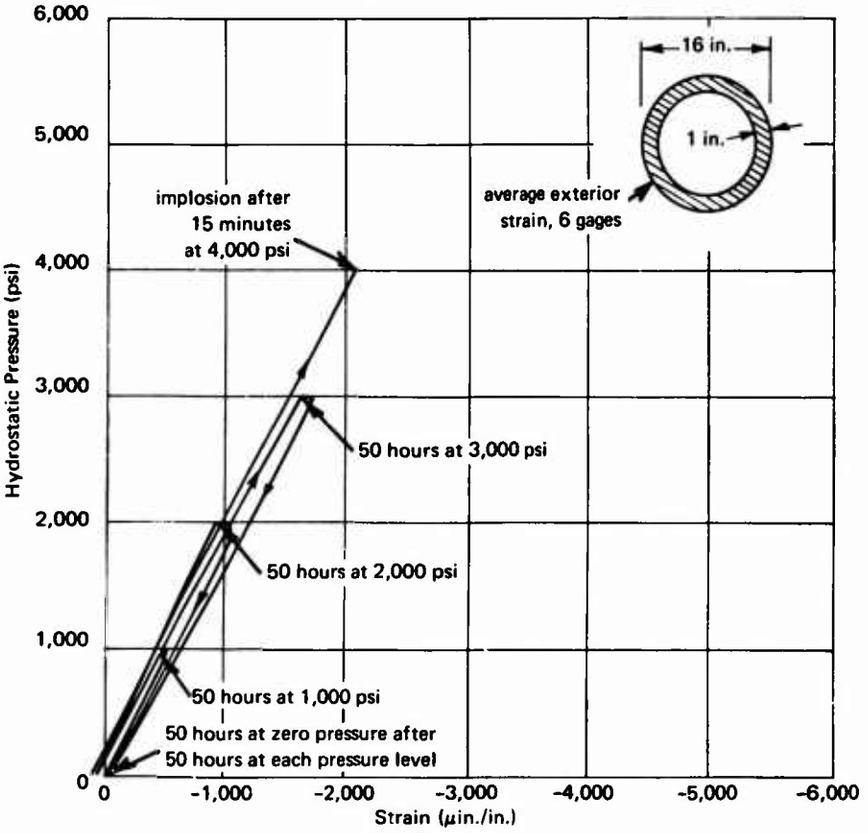

(b) Exterior.

Figure 14. Strain behavior of sphere H under cyclic loading; $t/D_o = 0.063$.

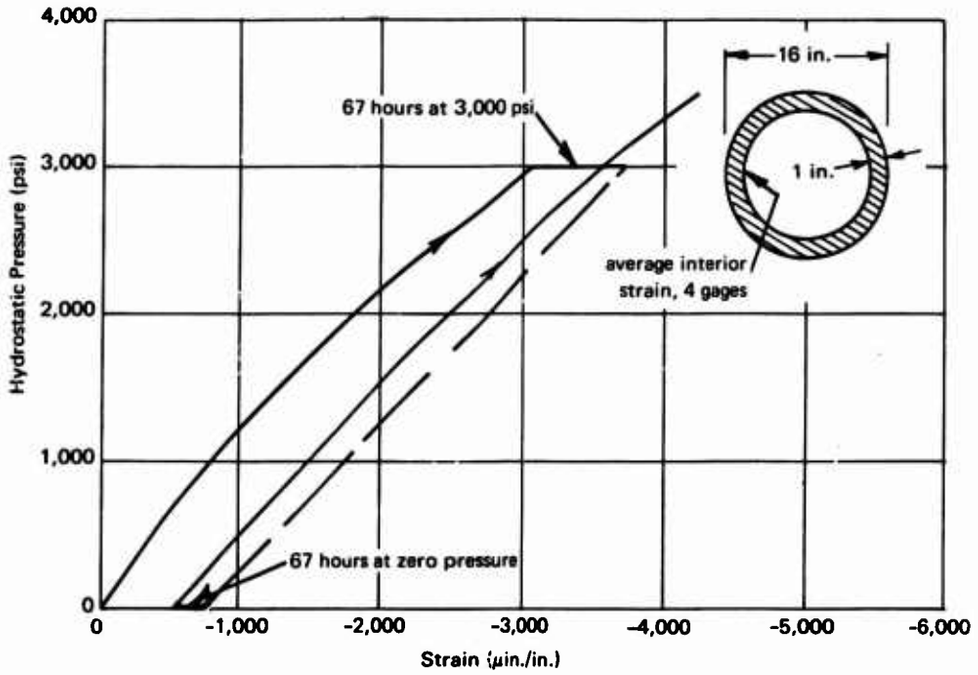

Figure 15. Interior strain versus hydrostatic pressure for a regular-concrete sphere[1] under cyclic loading; $t/D_o = 0.063$.

The implosion pressure for sphere F was 4,130 psi; this pressure was 86% of the average implosion pressure for the PIC spheres (A, B, and I) with a thin epoxy joint. Figure 18 shows that the decrease in implosion pressure due to the presence of the joint compared reasonably well to that of regular-concrete spheres with joints of similar relative stiffnesses.[9] Relative stiffness of a joint was defined as:

$$R = \frac{E_r A_r}{E_c A_c}$$

where R = relative stiffness

E_r = modulus of elasticity of ring joint material (psi)

A_r = cross-sectional area of ring joint (in.^{2})

E_c = secant modulus of elasticity of concrete (or PIC) to $\frac{1}{2} f'_c$ (psi)

A_c = area of concrete replaced by the ring joint (in.^{2})

The aluminum joint used on sphere F had a relative stiffness of 3.80.

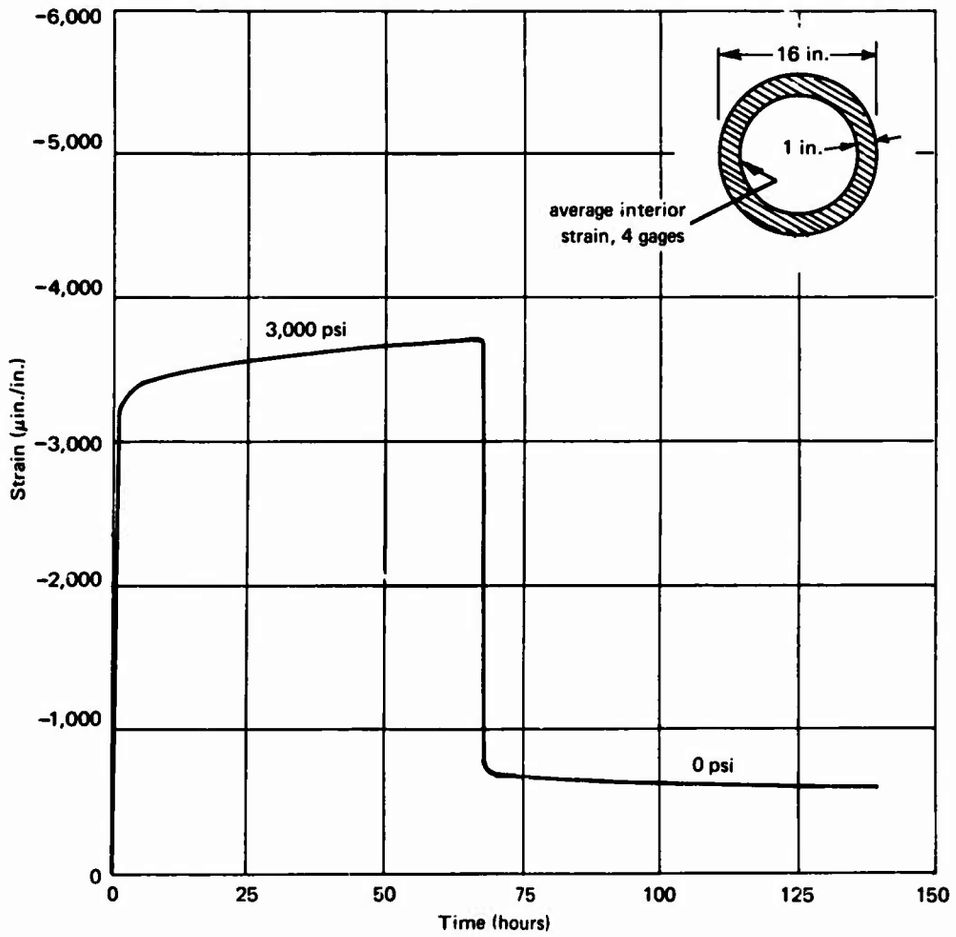

Figure 16. Interior strain versus time for a regular-concrete sphere[1] under cyclic loading; $t/D_o = 0.063$.

The strain behavior for sphere F is shown in Figures 19 and 20 along with the behavior for the PIC spheres with a thin epoxy joint. The aluminum joint changed the deformation pattern of the hemisphere sections from that of a sphere with a thin epoxy joint. However, the aluminum joint did not affect the strain behavior of the PIC sphere as significantly or severely as aluminum joints affected regular-concrete spheres. Actually, the strain behavior of sphere F compared quite well with that of a regular-concrete sphere having a fiber glass joint.[9] The fiber glass joint (Figure 18) had a relative stiffness of approximately 1.0, which was equivalent to the stiffness of the concrete hull.

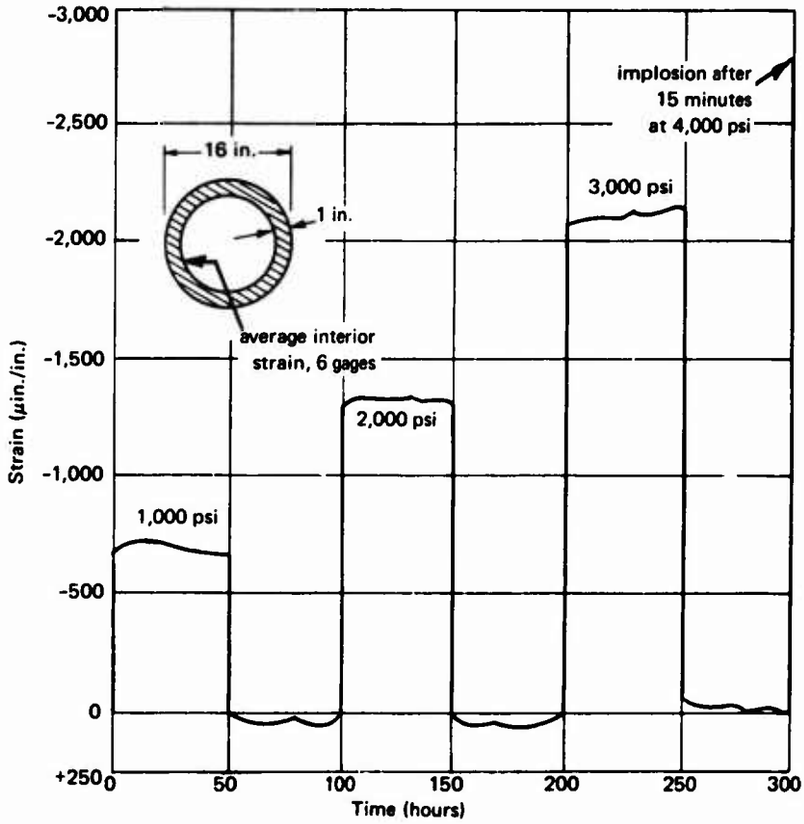

(a) Interior.

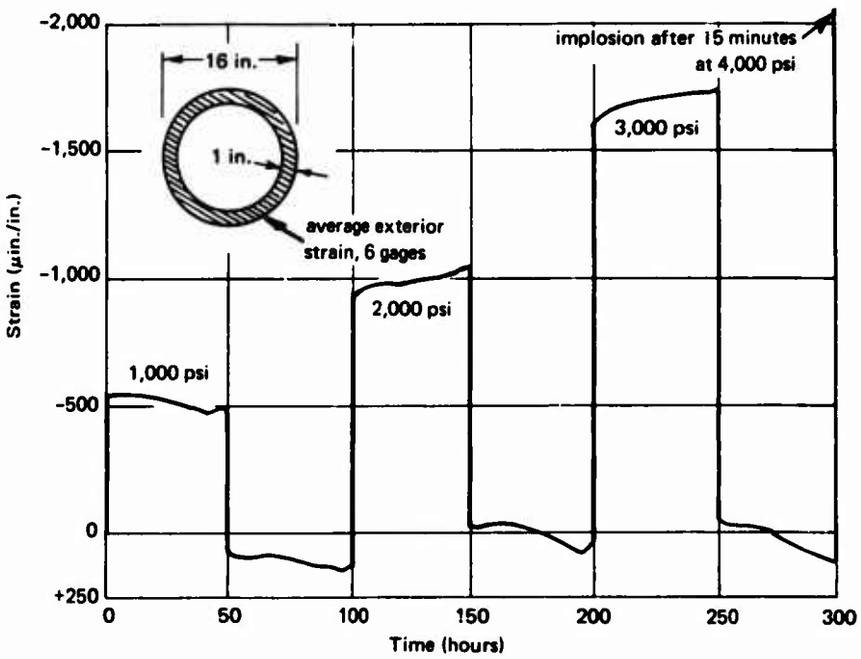

(b) Exterior.

Figure 17. Strain behavior of sphere H under cyclic loading; $t/D_o = 0.063$.

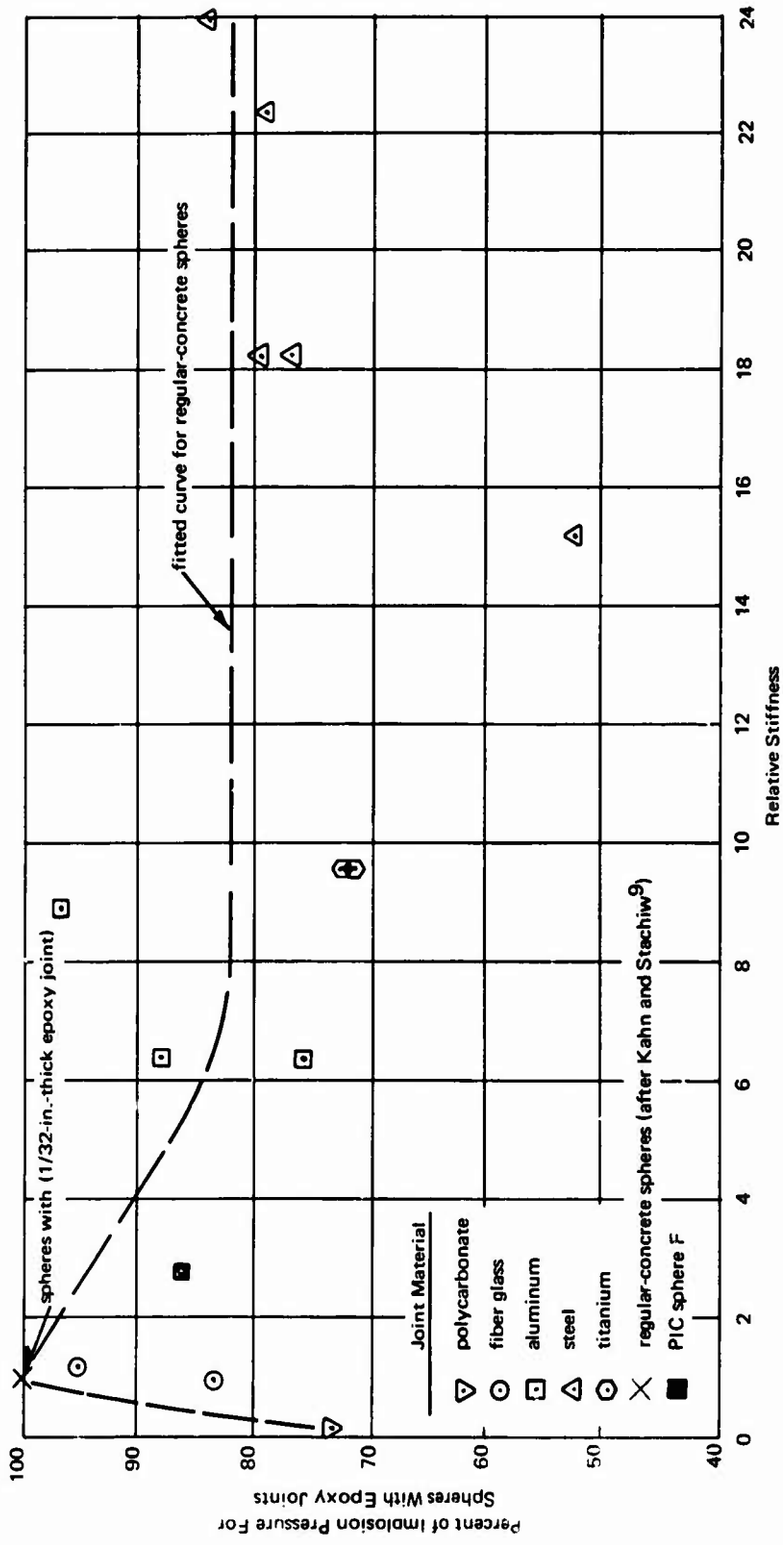

Figure 18. Comparison of implosion behavior of sphere F with regular-concrete spheres having mechanical joints.

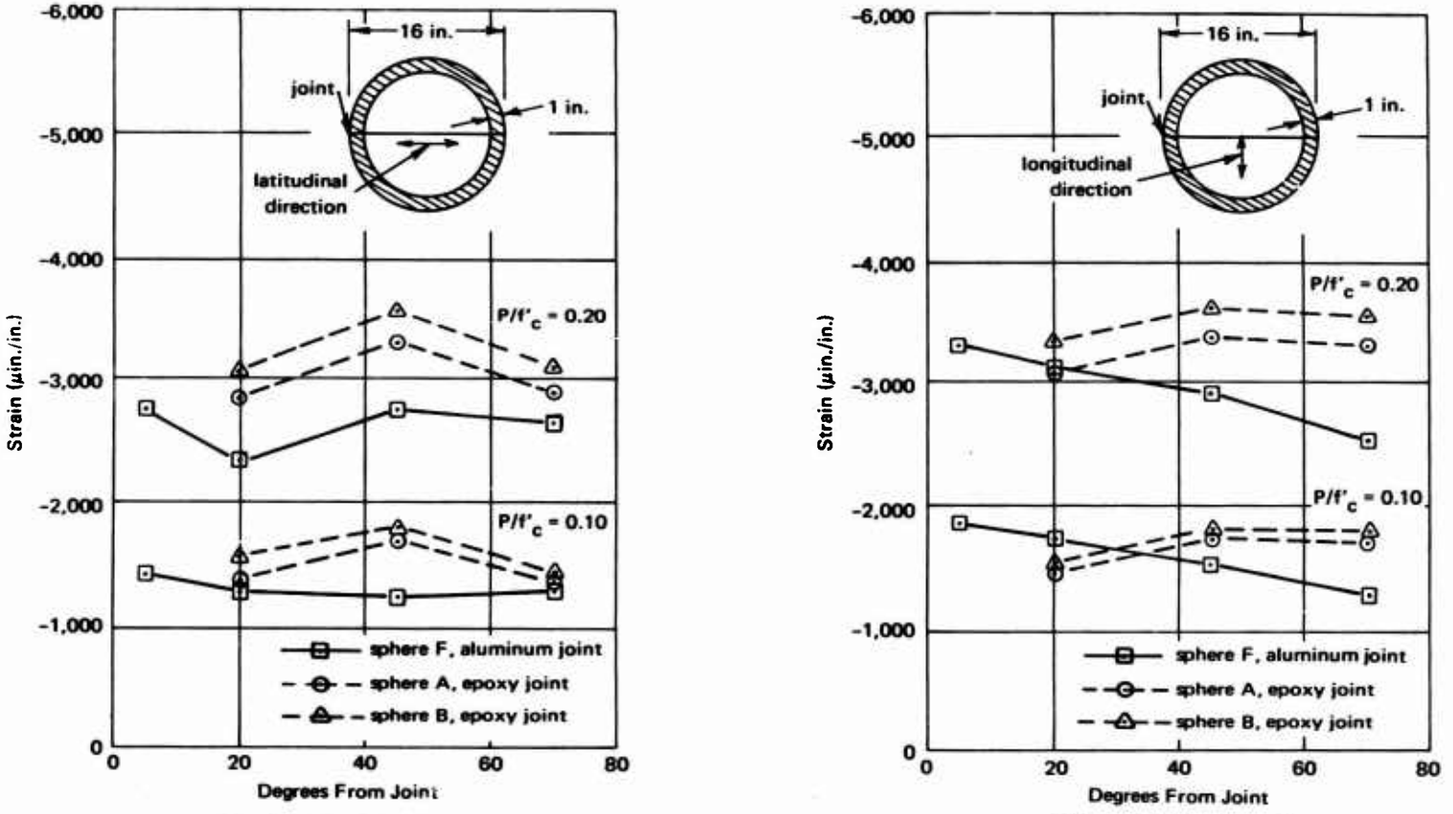

(a) Latitudinal direction.

(b) Longitudinal direction.

Figure 19. Interior strains of sphere F.

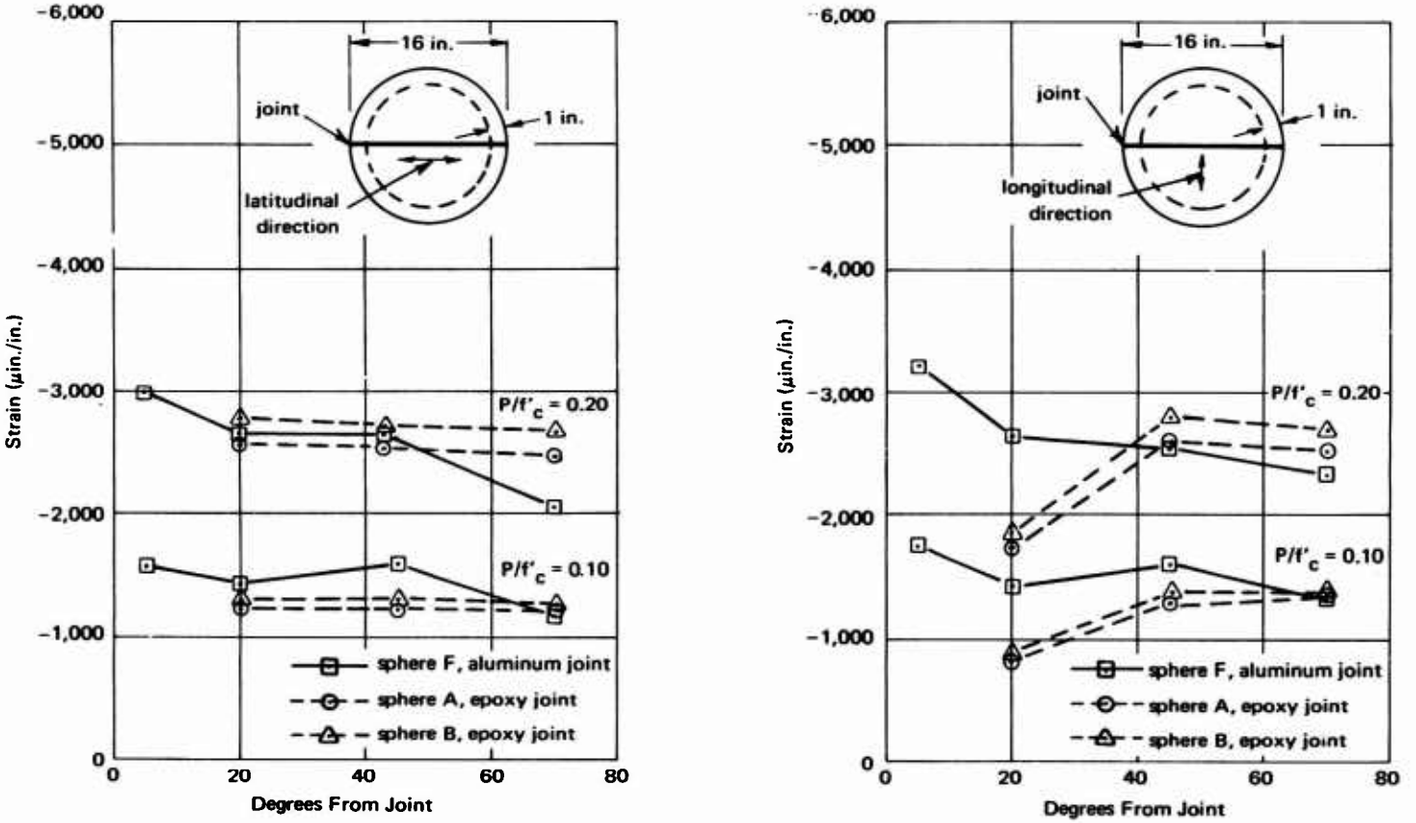

(a) Latitudinal direction.

(b) Longitudinal direction.

Figure 20. Exterior strains of sphere F.

The aluminum joint on the PIC sphere had a mating surface with the hull that was beveled; this was unlike the joints on the regular-concrete spheres which had flat mating surfaces. From the strain data it is evident that the beveled mating surface helped the joint appear less stiff to the PIC sphere by reducing the high bearing stresses on the interior edge. The flat mating surface produced high bearing stresses in the regular-concrete spheres. Hence, the beveled joint design was found to be an improvement over the joint design used by Kahn and Stachiw.[9]

DISCUSSION

Strain

The observed strain behavior of the PIC spheres tested under short-term loading was compared to theoretical strain behavior as shown in Figure 21. Theoretical strains were computed using the following elastic theory expression[10]

$$\epsilon_x = \frac{\sigma_x}{E} - \frac{\nu}{E}(\sigma_y + \sigma_z) \qquad (1)$$

where ϵ_x = strain in tangential direction (in./in.)

σ_x, σ_y = stresses in tangential direction normal to each other (psi)

σ_z = stress in radial direction (psi)

E = modulus of elasticity (psi)

ν = Poisson's ratio

The stresses were computed from Lame's equations for spheres:

$$\sigma_x = \sigma_y = P_o \frac{r_o^3}{2r^3}\left(\frac{r_i^3 - 2r^3}{r_o^3 - r_i^3}\right) \qquad (2)$$

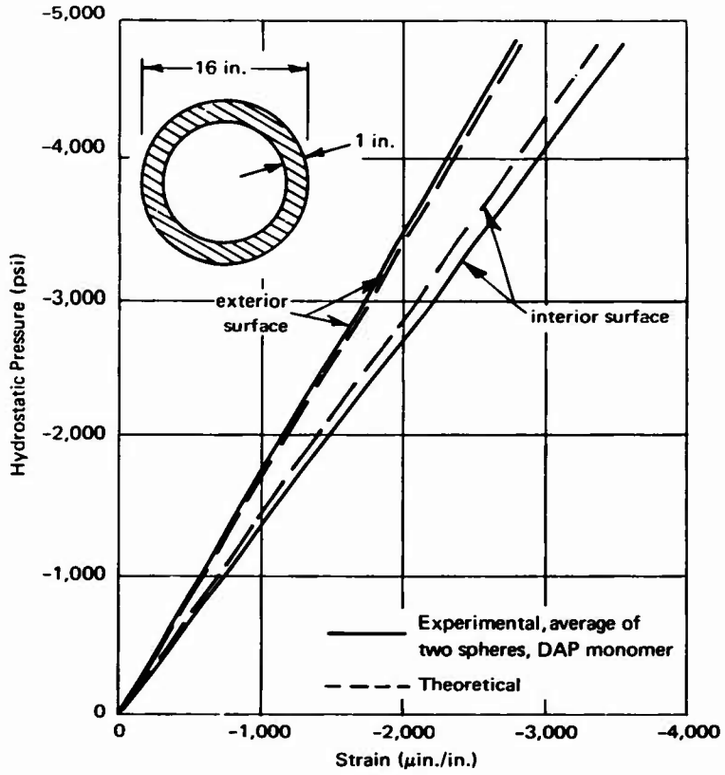

(a) $t/D_o = 0.063$.

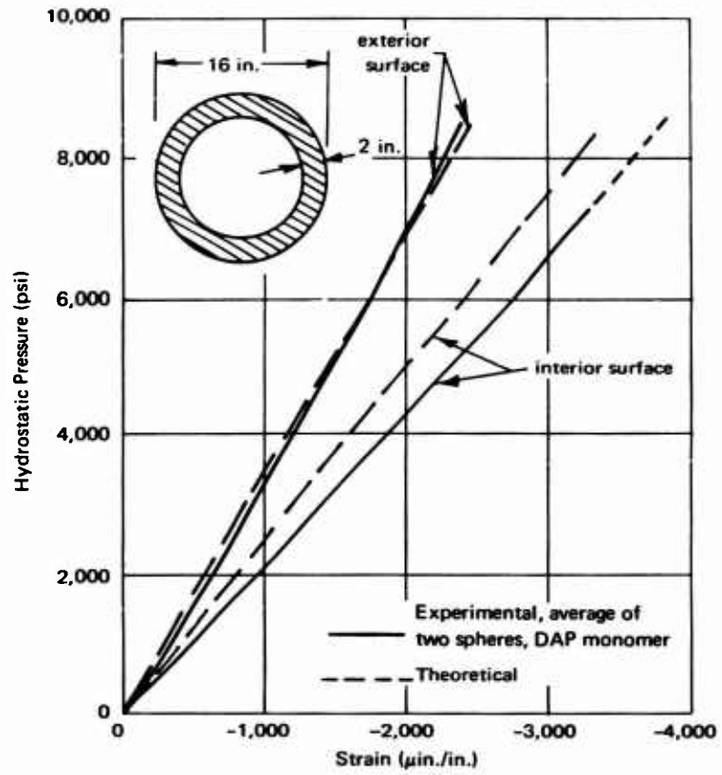

(b) $t/D_o = 0.125$.

Figure 21. Comparison of experimental to theoretical strain behavior for PIC spheres.

and

$$\sigma_z = -P_o \frac{r_o^3}{r^3}\left(\frac{r^3 - r_i^3}{r_o^3 - r_i^3}\right) \qquad (3)$$

where P_o = external pressure (psi)

r_o = external radius (in.)

r_i = internal radius (in.)

r = radius under consideration (in.)

At the exterior surface of the 1- and 2-inch-thick PIC spheres, observed and theoretical strain behavior compared exceptionally well. However, at the interior surface the experimental strain was greater than the theoretical by approximately 5 and 14% for the 1- and 2-inch-thick spheres, respectively.

Implosion Behavior

The implosion behavior for the spheres under short-term loading is shown in Figure 22 in terms of two ratios—implosion pressure to uniaxial compressive strength, P_{im}/f'_{PIC}, and wall thickness to outside diameter, t/D_o. Lame's elastic theory for spheres compared quite well with the experimental behavior. Equation 2 was used to predict the implosion pressures of PIC spheres by substituting r_i for r (because the interior wall was the location of the highest stresses), P_{im} for P_o, and f'_{PIC} for σ_x. Rearranging the equation yielded:

$$P_{im} = \frac{2}{3} f'_{PIC}\left[1 - \left(\frac{r_i}{r_o}\right)^3\right] \qquad (4)$$

where $r_i/r_o = 1 - 2(t/D_o)$

P_{im} = implosion pressure (psi)

f'_{PIC} = uniaxial compressive strength of 3x6-inch control cylinders (psi)

t = wall thickness (in.)

D_o = outside diameter (in.)

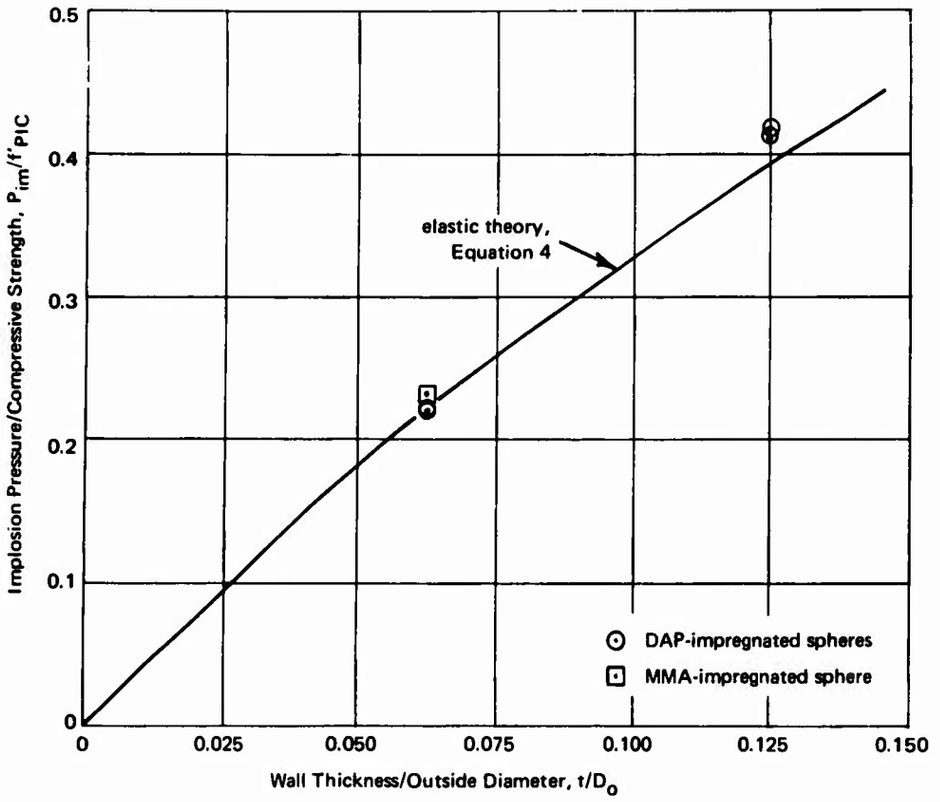

Figure 22. Comparison of implosion pressure for PIC spheres with elastic theory.

Applying Equation 4 to large spheres, say outside diameters of 20 feet or more, which have the same t/D_o ratios as the test specimens, design curves can be drawn to predict the operational depth in the ocean for PIC spheres. Figure 23 shows a family of operational depth curves; the reader may apply his own safety factor to the hull by relating allowable stress to the ultimate stress of 20,000 psi. For example, a neutrally buoyant sphere, t/D_o = 0.082, with a safety factor of 2 (allowable wall stress of 10,000 psi) would have a maximum operational depth of approximately 6,200 feet; if the safety factor was increased to 3, the maximum operational depth would be reduced to 4,100 feet. The reader must understand that the design curves are based on short-term test data, so the safety factor should compensate for the effect of long-term loading.

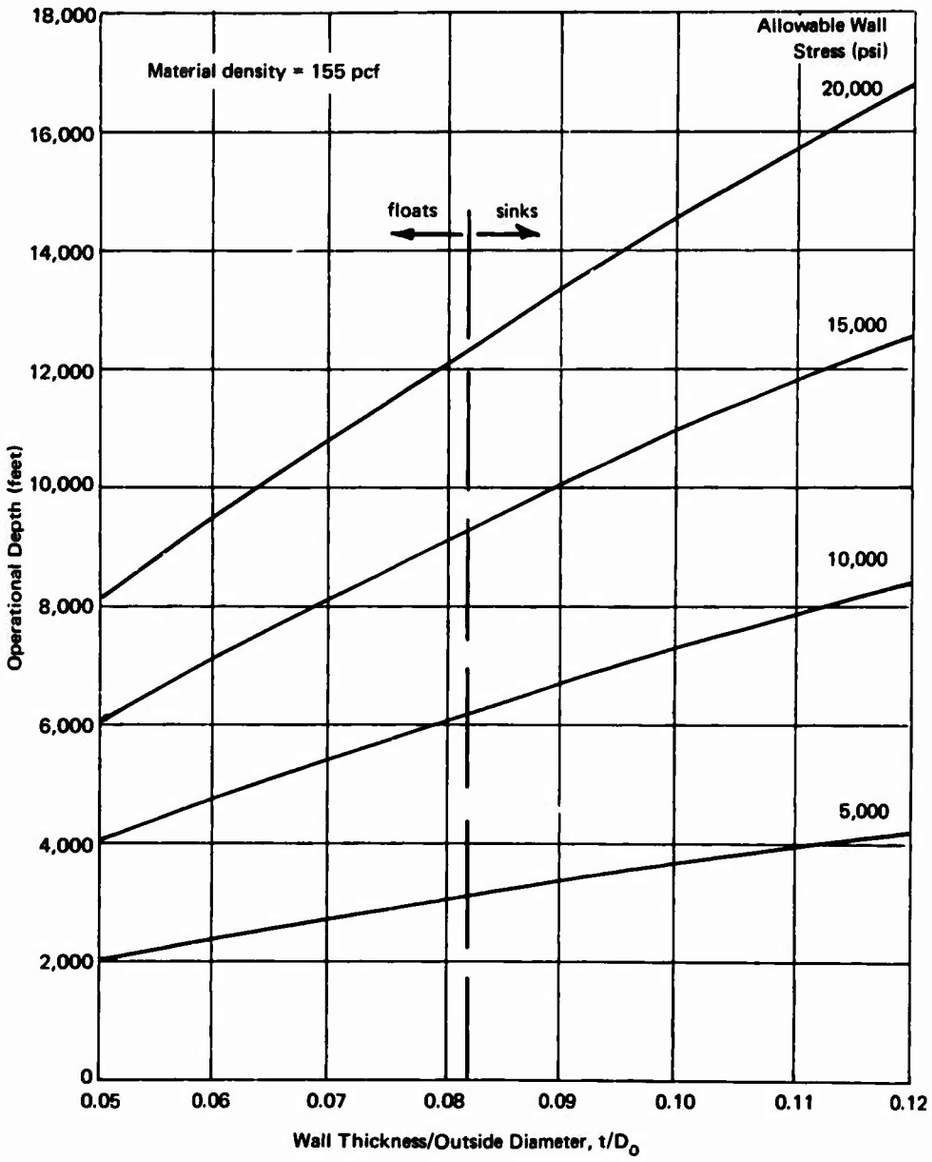

Figure 23. Operational depths for PIC spheres based on elastic theory.

Applications

Polymer-impregnated concrete appears to have a good future as a construction material for underwater structures. The behavior of PIC spheres in terms of high implosion pressures and linearly elastic response to various

hydrostatic loads demonstrated substantial improvements over regular-concrete sphere behavior; however, these improvements must be weighed against cost. The unit cost of PIC materials in a finished product is given in Reference 6 as being twice the unit cost of regular concrete. Using this information, Figure 24 was developed which compares the cost and depth of operation for buoyant spheres fabricated of PIC, concrete, and steel. The cost parameter is in terms of dollars per cubic foot of interior volume, making it a constant regardless of the actual size of the structure. (However, the comparison is estimated to be valid only for spheres with an outside diameter greater than 20 feet.) Regular-concrete spheres were found to be the most economical to a depth of approximately 3,000 feet, then PIC materials were cost effective to 4,100 feet, and for greater depths steel was the favored material, mainly because of strength, not cost. Other materials, such as aluminum or glass, were not considered in the comparison, because the cost of these materials is greater than steel.

The desirable features of PIC materials, such as watertightness and durability, can be incorporated into a regular-concrete structure without a major increase in cost by impregnating with a monomer a small portion of the outer wall of the structure. Only if increases in strength are required is it necessary to completely impregnate the wall with a monomer. Actually what is achieved by completely impregnating a sphere is an extended operational depth range—from 3,000 feet for regular-concrete spheres to 4,100 feet for PIC spheres.

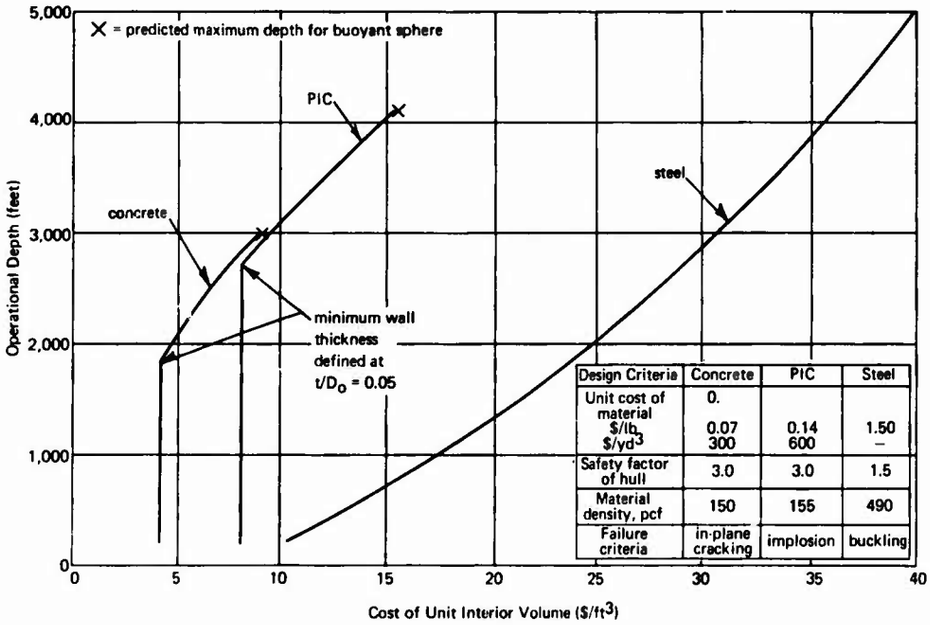

Figure 24. Cost comparison of buoyant spherical hulls with outside diameters greater than 20 feet.

PIC structures have the potential for a wide range of underwater applications, such as containment vessels for nuclear reactors or military structures to store materiel. Similar structures are feasible using regular concrete; however, by utilizing PIC materials, the structures could operate at deeper levels, would be less permeable to seawater, and could possess better durability characteristics than regular concrete.

FINDINGS

1. Polymer-impregnated concrete (PIC) control cylinders, 3 x 6 inches, containing an average 8.4% by weight DAP monomer had an average compressive strength of 20,970 psi and a modulus of elasticity of 5.34×10^6 psi; these properties were an increase of 121 and 52%, respectively, over those of regular-concrete control specimens.

2. PIC spheres with an outside diameter of 16 inches and wall thicknesses of 1 or 2 inches (t/D_o ratios of 0.063 or 0.125, respectively) imploded at average pressures of 4,810 and 8,475 psi or simulated depths of 10,700 and 18,800 feet, respectively.

3. The 1-inch-thick PIC sphere with an operational aluminum joint at the equator imploded at 86% of the pressure for similar spheres with thin epoxy joints.

4. The PIC spheres consistently showed linearly elastic behavior under hydrostatic loading conditions of short-term, long-term, and cyclic pressure.

5. Predictions of strain behavior and implosion pressures for PIC spheres having t/D_o ratios between 0.063 and 0.125 can be made using classical elastic theory.

CONCLUSIONS

Polymer-impregnated concrete (PIC) spheres with an outside diameter of 16 inches and t/D_o ratios of 0.063 and 0.125 implode at pressures greater than similar regular-concrete spheres. This implies that spheres fabricated of PIC materials will ultimately operate at deeper levels in the ocean than regular-concrete spheres. It is projected that the maximum depth for buoyant PIC spheres will be approximately 4,000 feet, whereas the maximum depth for regular-concrete spheres appears to be 3,000 feet.

A cost comparison of spherical structures fabricated of PIC, regular concrete, and steel indicates that polymer-impregnated concrete is competitive with regular concrete and is substantially less expensive than steel.

REFERENCES

1. Naval Civil Engineering Laboratory. Technical Report R-517: Behavior of spherical concrete hulls under hydrostatic loading, pt. 1. Exploratory investigation, by J. D. Stachiw and K. O. Gray Port Hueneme, Calif., Mar. 1967.

2.———. Technical Report R-547: Behavior of spherical concrete hulls under hydrostatic loading, pt. 2. Effect of Penetrations, by J. D. Stachiw. Port Hueneme, Calif., Oct. 1967.

3.———. Technical Report R-588: Behavior of spherical concrete hulls under hydrostatic loading, pt. 3. Relationship between thickness-to-diameter ratio and critical pressures, strains, and water permeation rates, by J. D. Stachiw and K. Mack. Port Hueneme, Calif., June 1968.

4.———. Technical Report R-679: Failure of thick-walled concrete spheres subjected to hydrostatic loading, by H. H. Haynes and R. A. Hoofnagle Port Hueneme, Calif., May 1970. (AD 708011)

5.———. Technical Report R-696: Influence of length-to-diameter ratio on the behavior of concrete cylindrical hulls under hydrostatic loading, by H. H. Haynes and R. J. Ross. Port Hueneme, Calif., Sep. 1970. (AD 713088)

6. Brookhaven National Laboratory. Report BNL 50134: Concrete-polymer materials. First topical report, by M. Steinberg, et at. Upton, N. Y., Dec. 1968. (Also Bureau of Reclamation, GEN. REP.-41, Denver, Col.)

7.———. Report BNL 50218: Concrete-polymers materials, 2d topical report, by M. Steinberg, et al. Upton, N. Y., Dec. 1969. (Also Bureau of Reclamation, Rec OCE-70-1, Denver, Col.)

8.———. Report BNL 50275: Concrete-polymer materials, 3d topical report, by J. T. Dikeou, et al. Denver, Col., Jan. 1971. (Also Bureau of Reclamation, Rec ERC-71-6, Denver, Col.)

9. Naval Civil Engineering Laboratory. Technical Report R-735: The influence of stiff equatorial rings on concrete spherical hulls subjected to hydrostatic loading, by L. F. Kahn and J. D. Stachiw. Port Hueneme, Calif., Aug. 1971.

10. R. J. Roark. Formulas for stress and strain, 4th ed. New York, McGraw-Hill, 1965, pp. 432.